© 2018. Published by The Company of Biologists Ltd.

Lipid-dependence of Target Membrane Stability during Influenza Viral Fusion

Sourav Haldar, Elena Mekhedov, Chad D. McCormick, Paul S. Blank and Joshua Zimmerberg*

Section on Integrative Biophysics, Eunice Kennedy Shriver National Institute of Child Health and Human Development, Bethesda, Maryland 20892, USA

* Correspondence and requests for materials should be addressed to J.Z. (email: joshz@helix.nih.gov)

Key words: spontaneous curvature, membrane, fusion, virus, poration

Journal of Cell Science • Accepted manuscript

JCS Advance Online Article. Posted on 2 July 2018

ABSTRACT

While influenza kills about a half million people each year, even after excluding pandemics, there is only one set of antiviral drugs: neuraminidase inhibitors. Using a new approach utilizing giant unilamellar vesicles and infectious X-31 influenza virus and testing for the newly identified pore intermediate of membrane fusion, we observed ~30 - 87 % poration as a function of lipid composition. Testing the hypothesis that spontaneous curvature (SC) of the lipid monolayer controls membrane poration, our Poisson model and Boltzmann energetic considerations suggest a transition from a leaky to a non-leaky fusion pathway depending on the SC of the target membrane. When the target membrane SC is below ~ -0.20 nm^{-1} fusion between influenza virus and target membrane is predominantly non-leaky while above that fusion is predominantly leaky, suggesting that HA catalyzed topological conversion of target membranes during fusion is associated with a loss of membrane integrity.

Journal of Cell Science • Accepted manuscript

INTRODUCTION

While most medical research aimed at reducing the impact of the influenza virus is focused on vaccines, anti-viral therapeutic strategies should not lag behind. The crucial stage of infection is the moment when the viral genome first enters the cytoplasmic space to begin infection – the fusion of the viral and endosomal membrane of a cell (White and Whittaker, 2016). Merging of two membrane-enclosed compartments is a ubiquitous event in biology, crucial to fertilization, exocytosis, bone and muscle development, intracellular trafficking and viral infection. The underlying biophysical determinants in these diverse processes are the same - the fusion of the mostly phospholipid bilayers that comprise the membranes. Enveloped viruses offer the experimenter easily purified compartments with well-defined fusion-enabling proteins. Specialized proteins on the viral membrane catalyze the merger of viral and cellular membranes. For influenza virus, fusion between viral and endosomal membranes is mediated by the surface glycoprotein haemagglutinin (HA) triggered by a decrease in endosomal pH that induces HA conformational change. Although influenza is a global health concern, one of the most widely studied viruses, and considered a paradigm for biological fusion, molecular details about the influenza haemagglutinin-mediated fusion remain elusive (Hamilton et al., 2012; Smrt and Lorieau, 2017).

HA-mediated fusion is hypothesized to occur through a stalk-pore pathway (Chernomordik, 1996; Chernomordik et al., 1997, 1999, 2006; Chernomordik and Zimmerberg, 1995; Chlanda et al., 2016; Gui et al., 2016). According to this model, viral and target (endosomal) membranes form an intermediate in which the proximal monolayers are merged but the distal monolayers remain intact. This process is referred to as hemifusion and the intermediate is referred to as a ‘stalk’ (Chernomordik et al., 1997; 1999; 2006). Subsequently, the stalk develops into a

Journal of Cell Science • Accepted manuscript

'hemifusion diaphragm' which then breaks open to form a fusion pore that connects these two membrane-bound compartments through an aqueous pathway. The hallmark of the stalk-pore hypothesis is that there is only one connection between the two membranes through a lipidic channel and the contents enclosed within fusing membranes never leak into the aqueous environment, consistent with the presumed fact that exocytotic fusion is leak-free (Palade, 1975). However, several experiments from different laboratories (Bonnafous and Stegmann, 2000; Frolov et al., 2003; Shangguan et al., 1996) and mathematical modeling (Katsov et al., 2006; Muller et al., 2003) suggest that fusion mediated by influenza HA is leaky, i.e., the target membrane integrity is compromised. Leakage of entrapped soluble markers can occur from a target liposome during fusion with influenza virus (Shangguan et al., 1996). Electrophysiological measurements show that target membrane permeability changes occur during early stages of complete HA-mediated fusion (Frolov et al., 2003). Monte Carlo simulation studies suggested that an elongated stalk can destabilize fusing membranes and promote hole formation in the vicinity of the stalk (Katsov et al., 2006; Muller et al., 2003). High resolution cryo-electron microscopy studies of intermediate hemifusion-structures of influenza virus and virus like particles (VLP) with liposomes (target membranes) revealed discontinuities in the target membranes (liposomes) and the existence of membrane edges, thus providing an ultrastructural reality for physiological leakage experiments (Chlanda et al., 2016; Lee, 2010). Clearly, one of the central tenants of the stalk-pore model, leak-free fusion, is not always a feature of HA-mediated fusion. Alternate models featuring leakiness of the target membrane are the current focus of this field.

Historically, one way to distinguish between lipidic models for membrane fusion is through predictions of the dependence of fusion upon lipid composition (Chernomordik, 1996; Chernomordik and Zimmerberg, 1995). Cryo-electron microscopy revealed that the target

Journal of Cell Science • Accepted manuscript

membrane rupture frequency is dependent on the target membrane cholesterol concentration such that at 40 % cholesterol (mol fraction) the rupture frequency was low and at 0 or 16 % cholesterol the rupture frequency was as high as 50 % of all fusion intermediates (Chlanda et al., 2016). This differential effect of cholesterol on membrane rupture was interpreted as a curvature-dependent branch point in the influenza haemagglutinin-mediated hemifusion pathway leading to either the canonical 'hemifusion-stalk' or a new proposed pathway: 'rupture-insertion'. Since the energy of the stalk intermediate is low at negative spontaneous curvature of the contacting monolayers (Chlanda et al., 2016; Ryham et al., 2016), we posit that when target membranes contain lipids with high negative spontaneous curvature of the contacting monolayers (for example, a high cholesterol concentration, comparable to that observed in endosomal membranes) the non-leaky 'hemifusion-stalk' pathway is preferred whereas in the case of low negative spontaneous curvature the leaky 'rupture-insertion' pathway is preferred, implying that under suitable compositions lipid mixing (lipidic junctions) can be accompanied by leakage of soluble contents. A simple prediction of this hypothesis is that the same degree of poration (leakage) should be seen in membranes with lipid compositions of similar spontaneous curvature independent of the specific chemical nature of their constituent lipids. To better understand the lipid dependence, we thus set out to experimentally test this prediction using a variety of lipid compositions. Using different lipid combinations (POPC and varying mole percent of Cholesterol, POPE or DOG) with the same estimated spontaneous curvature of the target membrane (see Table 1), we show that poration of the target membrane induced by influenza virus is modulated by the physical elastic properties of the target membrane, not merely the level of cholesterol as previously shown (Chlanda et al., 2016). These results are consistent with the hypothesis that the energy landscape of fusion can proceed via two co-existing pathways to completion: stalk-pore or rupture-insertion. A data-driven

Journal of Cell Science • Accepted manuscript

Poisson model and Boltzmann energetic model are consistent with the importance of the spontaneous monolayer curvature of the target membrane.

RESULTS

Concept of the poration assay

Existing *in vitro* biophysical methods, such as bulk fusion between virus and liposomes in a cuvette or fusion between labelled virus and a supported bilayer (Hamilton et al., 2012) are not suitable for monitoring lipid transfer (hemifusion) and content leakage simultaneously. While it is possible to accomplish such a task using a HA-expressing cell and a red blood cell (RBC) fusion model system (Frolov et al., 2003), one cannot modulate the biophysical properties of target membranes easily (RBC in this case). To overcome such limitations, we adopted an assay (Bleicken et al., 2013) that utilizes giant unilamellar vesicles (GUV) and an influx of aqueous dye (Fig. 1A). Using this assay, we monitor leakage of the target membrane during low pH-induced interactions of influenza virus X-31 to GUVs. Unlike conventional bulk leakage assays based on fluorescence spectroscopy where content leakage (flux through pores) and content transfer (from one vesicle to another) are often indistinguishable (Bao et al., 2016), our microscopy-based assay provides a direct measure of leakage as influx of aqueous dye at the single vesicle level.

Our assay is based on the strategy that while all fusion events between a viral particle and a GUV will result in lipid mixing, an influx of soluble dye will result only when an aqueous pathway arises between the inside of the GUV and the external medium (Fig. 1A). The optical sectioning of confocal microscopy allowed visualization of the dark background within the inside

Journal of Cell Science • Accepted manuscript

of the GUV even in the presence of soluble dye outside. First, to establish that the assay responds to poration of GUV membranes independently of membrane fusion or viral exposure, we incubated GUV with melittin, a well characterized pore-forming amphipathic peptide (Lee et al., 2008). An influx of Alexa-Fluor 488 occurred when melittin was introduced to a suspension of GUV (Fig. 1B), illustrating that membrane poration can be monitored by the influx of soluble dye. Almost 100 % of vesicles exhibited influx when melittin was added to a suspension of POPC GUV at 1:50 peptide-to-lipid ratio.

To monitor lipid mixing between influenza virus X-31 and target membranes, GUV-virus units were monitored using confocal scanning fluorescence microscopy prior to lowering pH and after the pH change. At pH 7.4, GUV incubated with R-18-labelled virus exhibited binding of viral particles to the GUV (Fig. 1C). At pH 7.4 there was no influx of Alexa-488 indicating there is no leakage in the presence of virus at neutral pH. When the pH was changed from 7.4 to 5.0 in a sample of virus/GUV, the intensity of R-18 on GUV membranes, upon subsequent observation, increased by ~ 400 % (Figs. 1C and 1D). The increase is due to the transfer of R-18 molecules from viral to GUV membranes upon lipid mixing at low pH and consequent dequenching of R-18 following dilution within the two-dimensional GUV membrane. This is equivalent to the increase in intensity observed in cuvette-based measurements demonstrating lipid mixing from viral to target GUV membranes (Arbuzova et al., 1994).

To monitor GUV poration, water soluble Alexa-488 was dissolved in the solution external to the GUV. Some, but not all the vesicles which displayed lipid dye transfer from the viral membrane upon lowering pH also exhibited an influx of Alexa-488 (middle panel of Fig. 1C). Conversely, all of the vesicles which exhibited poration also displayed lipid dye transfer. Several observations indicate that this is the correct interpretation of influx of aqueous dye. First, the ratio

Journal of Cell Science • Accepted manuscript

of intensities of the green dye inside and outside of the GUV is generally close to 1 suggesting the target vesicles became leaky while fusing with X-31 influenza virus. Second, this influx is not due to an osmotic imbalance (internal and external solutions were iso-osmolar), and incubation of GUV in the absence of virus at 37 ^{0}C and (or) incubation at pH 5, under our experimental conditions did not lead to either lipid mixing or soluble dye entry. Third, the degree of poration did not depend on the kind of virus, whether laboratory-prepared fresh virus or egg-grown, freeze-thawed virus, both exhibited similar degrees of poration. This is an important control as it was thought only egg-grown, freeze-thawed virus can induce permeability changes in the target membrane (Young et al., 1983). Fourth, the influx was not dependent on Alexa-488. In control experiments where sulforhodamine B was introduced along with Alexa-488, influx to the same extent was observed.

Variation of poration with target membrane spontaneous curvature

Our hypothesis that the lowest energy pathway through the energetic landscape for membrane remodeling is dependent upon the spontaneous curvature of the monolayer of the target membrane predicts a significant decrease in poration with target lipid compositions favoring negative curvature. To test this prediction, GUVs were prepared in which a fraction of the POPC was gradually replaced with reciprocal fractions of POPE, cholesterol, DOG, or combinations thereof (described in Table 1). Poration of these vesicles were monitored under identical conditions. The fraction of porated vesicles decreased with increases in non-bilayer lipid mole fractions in GUVs and consequent decrease in PC mole fraction (Fig. 2A).

If the decrease in leakage is due to an increase in negative spontaneous curvature, then individual lipid series should converge using a transformation to the spontaneous curvature axis.

Journal of Cell Science • Accepted manuscript

Spontaneous curvature of GUVs with varying amount of Cholesterol, POPE or DOG spanned the same range from $-0.022\ nm^{-1}$ to $-0.305\ nm^{-1}$. As expected, the individual lipid series tend to converge on the curvature axis (Fig. 2B). The fraction of porated vesicles decreased to less than 0.3 at 60 mol % cholesterol (estimated spontaneous curvature $-0.303\ nm^{-1}$) compared to > 0.8 with no cholesterol (estimated spontaneous curvature $-0.022\ nm^{-1}$). To test whether this is a curvature-mediated effect we evaluated poration in GUVs with 27 mol % DOG such that the total spontaneous curvature is $-0.303\ nm^{-1}$ (see Table 1). Poration with DOG was similar to poration of cholesterol-containing vesicles (Fig. 2B; filled circles cholesterol and squares DOG). Corresponding data for POPE containing vesicles could not be obtained as GUVs with very high POPE were not stable under our experimental conditions. GUV diameters varied from ~7 to 28 µm (12 ± 6 µm; mean ± sd). No dependence of leakage (in/out intensity ratio of Alexa-488) on the size of the vesicles was observed. Although the individual series deviated from each other on the spontaneous curvature axis, an overall decreasing trend in poration with increasing negative spontaneous curvature was observed in every case (Fig. 2B).

Interpreting leakage using a Poisson model

To establish a quantitative relationship between the degree of poration and spontaneous curvature we developed a Poisson leakage model. In our system, several viral particles interact with one GUV; we postulate that some viral particles induce poration or leakage via one or more "leakage machines". In other words, the GUV viral particle system has reserve capacity – one viral particle or viral particle component may be sufficient for leakage, but more than one viral particle or viral particle components may participate in the observed leakage. Previously, a Poisson model was developed that described the consequences of reserve capacity in calcium-triggered vesicle fusion (Coorssen et al., 1998; Blank et al., 2001; Vogel et al., 1996; Zimmerberg et al., 2000). We

Journal of Cell Science • Accepted manuscript

therefore applied a similar model to our data. In analogy with the Poisson analysis of the extent and kinetics of calcium-triggered cortical vesicle fusion to plasma membrane, we postulate the existence of a 'leakage machine' responsible for poration during lipid mixing. The model relates the extent of leakage with the number of leakage machines, and by experimental dependency, with the spontaneous curvature of the target membrane. Using the Poisson distribution, we can identify the statistical element responsible for leakage. These will be termed 'leakage machines', and we identify an exponential relationship between the reserve capacity of the system and the spontaneous curvature. The leakage probability or observed leakage fraction, is defined by the following relationship:

$$L(< n >) = 1 - e^{-<n>}, \quad (1)$$

or $$< n > = -\ln(1 - L(< n >)), \quad (2)$$

where L(<n>) is the leakage probability or fraction of leaky vesicles observed and <n> is the Poisson distributed, mean number of leakage machines. By analogy with previous studies, (Coorssen et al., 1998; Blank et al., 2001; Vogel et al., 1996; Zimmerberg et al., 2000) we expected that the relationship between <n> and spontaneous curvature (SC) would be exponential. Therefore, we analyzed <n>, calculated from the leakage fraction, as a function of SC using the relationship $< n > = a * e^{b*SC}$, (3) where a and b are fitting parameters (see Table S1 of Supplementary Information). For every lipid composition (Table 1), leakage as a function of spontaneous curvature can be described using the postulated exponential dependence (Fig. 3).

To determine the dependence of energetics associated with poration on SC, we calculated the Boltzmann factor of our leakage data. The model assumes that the fraction of porated vesicles represents the probability of at least one lipid mixing event by the leaky pathway. Difference in

Journal of Cell Science • Accepted manuscript

energetics between the non-leaky and leaky pathways would govern the proportions of fusion events by these two pathways in the following manner. Given the probability of leakage L(<n>) ('rupture-insertion' pathway according to Chlanda et al., 2016) and the probability of no leakage NL(<n>) = 1 – L(<n>),(4) ('hemifusion-stalk' pathway, according to Chlanda et al., 2016), the Boltzmann factor relates the ratio of the two probabilities to the energy difference between the two states of the system. With ΔE defined as the energy difference between the non-leaky and leaky states of the system, the ratio of probabilities is:

$$\frac{L(<n>)}{NL(<n>)} = e^{\Delta E/k_B T},(5)$$

or

$$\ln\left(\frac{L(<n>)}{NL(<n>)}\right) = \Delta E/k_B T,(6)$$

Changes in energy, in units of $k_B T$ can be expressed using the Poisson model probabilities

$$\frac{\Delta E}{k_B T} = \ln\left(\frac{1-e^{-<n>}}{e^{-<n>}}\right) = \ln(e^{<n>} - 1),(7)$$

Expressing <n> as a function of SC models the relative energy relationship between the two pathways as a function of SC, $\frac{\Delta E}{k_B T} = \ln(e^{a*e^{b*SC}} - 1),(8)$

The values a = 2.0 and b = 5.2 were determined using the "all data" fit model of the relationship between leakage and SC (see Table S1 of Supplementary Information for details). The measured relative change in energy calculated from the data is then compared with the model relationship (Fig. 4). Note, the energy crossover point occurs at a spontaneous curvature of −0.20 nm^{-1}. This SC value agrees with the value determined from continuum model describing the relative energy of stalk formation as a function of spontaneous curvature (Chlanda et al., 2016).

Journal of Cell Science • Accepted manuscript

DISCUSSION

We developed a new assay that features detection of lipid dye mixing between a virus particle and its target membrane simultaneous with detection of aqueous dye mixing across the target membrane from the external solution, using confocal microscopy of single vesicles. Monitoring influx of aqueous dye achieved an optimal signal-to-noise ratio with no interference from photobleaching. This influx of soluble dye to GUV corresponds to edge formation in target membranes during their fusion with virus detected by phase-contrast cryo-electron microscopy (Chlanda et al., 2016). The interaction of influenza viral particles with the target GUV that leads to lipid mixing is modulated by the monolayer spontaneous curvature of the target membrane. Our data was well described using a Poisson model in analogy to calcium-triggered fusion. Boltzmann distribution analysis of our data shows a crossover point on the spontaneous monolayer curvature axis, beyond which the probability of poration events decreased significantly. The decrease in poration of the target membranes is consistent with the hypothesis that a switch in lipid mixing pathway from leaky 'rupture-insertion' to non-leaky 'hemifusion-stalk' is dependent on the spontaneous curvature of the target membrane (Chlanda et al., 2016). Our data is consistent with a crossover (Fig. 4) point ~ −0.20 nm^{-1} in agreement with a predicted value of −0.21 nm^{-1} for a membrane containing 31 mol % cholesterol (Chlanda et al., 2016). Interestingly, such a dependence of poration by influenza virus on monolayer spontaneous curvature was never observed in a bulk spectroscopic fusion assay (Shangguan et al., 1996).

There are primarily two hypotheses regarding membrane edge formation (variously termed as poration, rupture, or leakage) of the target membrane during influenza virus-mediated fusion. First, rupture could be secondary to adhesion of viral particles to target membrane, if the energy of attachment overcomes the membrane stability (Chlanda et al., 2016). Second, the leakage can

Journal of Cell Science • Accepted manuscript

be due to the insertion of a fusion peptide and consequent deformation of the target membrane as a 'collateral damage' (Blumenthal and Morris, 1999; Engel and Walter, 2008). There are several examples reported in the literature describing leakage from target membranes induced by the isolated fusion peptide. For example, a synthetic fusion peptide of the X-31 influenza virus deformed, changed permeability and eventually caused lysis or rupture of giant vesicles (Longo et al., 1997; Soltesz and Hammer, 1995) and caused content leakage from large unilamellar vesicles (Murata et al., 1992). Therefore, it is possible that leakage in our assay could be due to influenza fusion peptide-induced deformation of target GUV at low pH. In any event, to induce poration, the energy of the system must be greater than the line tension of the pore (Chernomordik et al., 1985). Line tension is defined as the energy penalty associated with forming a membrane edge to avoid exposing the hydrophobic parts of lipids to an aqueous environment. Since this edge has a highly bent lipid surface, it has been proposed that lipids with positive spontaneous curvature reduce line tension and facilitates pore formation, whereas the opposite happens with negative spontaneous curvature (Chernomordik et al., 1985; Karatekin et al., 2003). Therefore, the probability of detecting pores in membranes with high negative spontaneous curvature should be less since it would be an energetically demanding process. Our findings are consistent with this idea and suggest that there is a tradeoff between influenza fusion machinery (particularly the fusion peptide) induced deformation and lipid curvature-mediated line tension.

According to the curvature hypothesis, we expected the leakage percentage to follow identical trends on the curvature axis for different lipid compositions. However, they do not follow an identical trend, but deviate from each other and the predicted trend (Fig. 3). It is possible this feature of our data could be explained by other factors that are influenced by the lipid composition. Cholesterol has profound effects on several biophysical properties of lipid membranes pertaining

Journal of Cell Science • Accepted manuscript

to membrane elasticity such as fluidity, bending rigidity and lysis tension. These properties may vary among different lipid compositions (such as POPE and DOG) leading to identical spontaneous curvature. For example, elastic area compressibility as determined by micropipette aspiration is significantly different for cholesterol containing membranes than for POPE containing membranes at similar spontaneous curvature (Evans and Needham, 1986; Needham and Nunn, 1990). In other words, two lipid compositions could be identical in curvature space yet different in area compressibility or lysis tension space. Interestingly, it has been observed in a simulation study of SNARE-mediated fusion that POPE supports a leaky fusion pathway more than cholesterol, despite having similar negative spontaneous curvature, and the energy to nucleate a leakage pore is much higher in the presence of cholesterol than POPE (Risselada et al., 2014).

How general is the loss of membrane continuity, alternatively termed as membrane edge formation, during fusion? It has been noted that in addition to influenza several paramyxoviruses such as Sendai virus elicit change in cellular permeability during entry (Foster et al., 1980; Papanicolaou et al., 2012; Pasternak and Micklem, 1981) and some of the viral pathophysiology may be due to an alteration in cellular permeability. However, the biophysical underpinnings have not been deciphered. Membrane edge formation detected as permeability changes during protein-mediated fusion processes is increasingly recognized in the literature (Engel and Walter, 2008; Papanicolaou et al., 2012). Content leakage from target membrane is thought to be a consequence of membrane deformation during fusion steps. For example, content leakage from target membranes during SNARE-mediated fusion has been reported recently (Bao et al., 2016). It was previously suggested that SNARE mediated stalk expansion is leaky (Risselada and Grubmuller, 2012). Mitofusin-catalyzed mitochondrial fusion is associated with a permeability change in the mitochondrial membrane (Papanicolaou et al., 2012). Our general hypothesis is that during

Journal of Cell Science • Accepted manuscript

topological conversion of target membranes, the edges of pores are stabilized by specific proteins (such as the influenza fusion peptide) either surrounding the hydrophobic chains themselves or entering the bilayer to alter the energy landscape to promote bent lipidic intermediates. The GUVs used in this study are symmetric, *i.e*., the lipid compositions of the two leaflets are similar. Earlier studies have shown that the effect of spontaneous monolayer curvature on HA-mediated stalk formation and fusion is leaflet-specific (Chernomordik et al. 1997, 1998; Melikyan et al., 1997). When the spontaneous curvature of the contacting (proximal or cis) monolayers was increased by introducing lyso-phosphatidylcholine within the cis monolayer, stalk formation and full fusion was inhibited. However, decreasing spontaneous curvature by introducing oleic acid within the proximal monolayer promoted stalk formation and full fusion. Interestingly, when the spontaneous curvature of the distal or trans monolayer was increased by incorporating either lyso-phosphatidylcholine (Chernomordik et al., 1998) or chlorpromazine ((Melikyan et al., 1997), stalk formation was promoted. Leaflet specific modulation of spontaneous monolayer curvature on edge formation or poration in our assay remains to be understood. Since increasing the spontaneous curvature of the inner monolayer promotes stalk formation, we predict that poration or edge formation would diminish when lyso-phosphatidylcholine is introduced specifically within the inner leaflet of GUV (trans to virus). Future experiments with asymmetric GUVs will address this issue and will determine if the lipid compositional requirements are general for other phenomenon that show free edges of membranes, for example, vaccinia virus maturation ((Chlanda et al., 2009) and nuclear membrane organization (Shah et al., 2017).

Journal of Cell Science • Accepted manuscript

MATERIALS AND METHODS

Materials

1-palmitoyl-2-oleoyl-*sn*-glycero-3-phosphocholine (POPC), 1-palmitoyl-2-oleoyl-*sn*-glycero-3-phosphoethanolamine (POPE), Cholesterol, 1-2-dioleoyl-*sn*-glycerol (DOG) and Total Gangliosides Extract (TG) were obtained from Avanti Polar Lipids, Inc. (Alabaster, AL) and other chemicals were from Sigma-Aldrich (St. Louis, MO), unless mentioned. Stock solutions of POPC (13.15 mM), POPE (35 mM) and Cholesterol (20 mM) were made in $CHCl_3$ (Burdick & Jackson, Mexico City, Mexico, high purity solvent) and TG (5 mM) in Chloroform:Methanol:Water (65:35:8) and were stored in brown glass vials at −20 ^{0}C.

Preparation of Giant Unilamellar Vesicles (GUV)

Giant unilamellar vesicles were prepared by the gel swelling method as described previously (Weinberger et al., 2013). Briefly, to prepare GUVs of a specific lipid composition the required amount of lipid drawn from individual stock solutions was diluted into 200 µL of $CHCl_3$ to a concentration is 3.94 mM (3.35 mg/ml). The mixture was vortexed with ~10 µL of MeOH for ~2 min to avoid incomplete mixing and obtain a clear solution in $CHCl_3$. To this lipid mixture 10 µL of DiD (Invitrogen) was added (from a stock of 5 µM in DMSO) and vortexed for ~2 min. This lipid mixture (in $CHCl_3$) was then deposited on a plasma cleaned (using a Harrick plasma cleaner, Ithaca, NY) microscope cover glass, coated with 5 % (w/w in ddH_2O) Polyvinylalcohol (Merck Millipore). The organic solvent was evaporated by a gentle stream of nitrogen and followed by storing in high vacuum for 1 hour. The cover glass with the lipid film on was then transferred to a 30-mm tissue culture dish. 500 µL of PIPES buffer (1 mM EDTA, 1 mM HEDTA,

Journal of Cell Science • Accepted manuscript

10 mM PIPES, 100 mM KCl, pH 7.4 with ~200 mM sucrose) was added covering the entire surface of the cover glass and allowed to incubate for 30 min in the dark. After 30 min, the GUVs were harvested by gently tapping the sides of the dish, then gently drawing out using a 1 mL pipette without touching the surface and transferred to a 1.5 mL micro-centrifuge-tube. The GUV suspension was stored at 4 ^{0}C until further use. The total lipid concentration of GUV suspension was 1.35 mg/ml (1.58 mM). Typically, GUVs were made the same day of the experiment. To vary the spontaneous curvature systematically, POPC GUVs of varying concentrations of cholesterol, POPE or DOG (see Table 1) were prepared. Spontaneous curvatures of the target membranes for a given lipid composition were estimated using a mole fraction weighted summation of the spontaneous curvatures of the individual lipids (Table 1). The spontaneous curvatures of POPC, Cholesterol, POPE, and DOG used in the calculations are: −0.022 nm^{-1}, −0.494 nm^{-1}, −0.316 nm^{-1}, and −0.99 nm^{-1}, respectively (Kollmitzer et al., 2013; Szule et al., 2002). Every GUV composition included 5 mol % of TG as the receptor lipid for HA.

Preparation and purification of influenza virus A/Aichi/68 (X-31)

Egg-propagated and sucrose gradient-purified influenza A virus (A/Aichi/68) was purchased from Charles River Laboratories (Wilmington, MA). MDCK (purchased from ATCC (NBL-2) (ATCC® CCL-34™) cells were seeded on 8x10 cm Petri dishes (2x10^{6} cells/dish) one day prior to infection. Confluent cells were washed three times with serum-free SFM4 MegaVir medium (Thermo Fisher Scientific, Inc.) and inoculated with 50 µL of A/Aichi/68 (50% egg-infective doses per mL [EID50]: $10^{9.5}$) in 5 mL of serum-free SFM4 MegaVir medium. After a 45-minute incubation at 37 °C, 20 mL of SFM4 MegaVir medium (supplemented with L-glutamine, primocine and 2 µg/ml of tosylsulfonyl phenylalanyl chloromethyl ketone (TPCK)-treated trypsin (Sigma)) were added to each dish. 48 hours post-infection the culture medium was clarified by

Journal of Cell Science • Accepted manuscript

centrifugation at 1,000 × g for 10 min at 4 °C. Subsequently, the supernatant was layered onto a 3 ml 30 % (wt/vol) sucrose-KHE (100 mM KCl, 10 mM HEPES (pH 7.4), 1 mM EDTA) cushion and centrifuged at 200,000 × g for 2 h at 4 °C in a Beckman Optima XL 100K centrifuge using a 50.2Ti rotor (Beckman Coulter, Fullerton). The concentrated virus was re-suspended in KHE buffer and centrifuged at 100,000 × g for 30 min at 4 °C in Beckman Coulter OptiMax centrifuge, using TLA 100.3 rotor. The pellet was diluted in KHE buffer and incubated with Octadecyl Rhodamine B Chloride (R-18, Thermo Fisher Scientific, Waltham, MA) for 30 min in the dark with mild shaking (3 µL of 1 mg/mL of R-18 in DMSO to ~400 µL of viral suspension) and layered onto 10 –40 % continuous Optiprep-KHE gradient, centrifuged at 200,000 × g for 2 h at 4 °C in a Beckman Optima XL 100K centrifuge using a SW55 rotor (Beckman Coulter, Brea, CA). The banded virus was collected, diluted in KHE buffer, pelleted and centrifuged at 100,000 × g for 30 min at 4 °C in Beckman Coulter OptiMax centrifuge, using TLA 100.3 rotor and resuspended in 300 mL KHE buffer. Total protein content of a virus preparation was determined using the BCA assay (Thermo Fisher Scientific, Waltham, MA). R-18 labelling did not cause any visible damage as visualized by negative staining by electron microscopy.

GUV-virion lipid mixing and poration of GUV membranes

The GUV-based lipid mixing, and leakage assay is schematically described in Fig. 1. R-18 labelled X-31 virus was incubated with GUVs of defined compositions (Table 1). For a typical fusion experiment, 100 µL of the GUV suspension is incubated with X-31(Charles River or lab grown, ~9 µg of total protein) virus (sonicated for 1 min in a Branson bath sonicator prior to use) in a 1.5 mL micro-centrifuge-tube at 37 ^{0}C for 30 min. 200 µL of Alexa Fluor 488 (Invitrogen, 6 µM in PIPES buffer with 200 mM sucrose), and 200 µL of PIPES buffer (with ~200 mM glucose)

Journal of Cell Science • Accepted manuscript

were added to achieve a final concentration of ~2 μM Alexa Fluor 488. The mixture was vortexed for 2 min and 6 μL of 0.5 M citric acid was added to change the pH to 5, again vortexed for ~2 min, incubated for another 10 min at 37 ^{0}C for end-point measurements. While the GUV-virus mixture was incubating, 500 μL of a 5 mg/mL β-casein solution was added to a delta-TPG 0.17 mm dish (Bioptechs, Butler, PA) allowed to sit for 10 min to passivate the glass surface, and then washed 10 times with ddH_2O. The GUV-virus suspension was then transferred to this imaging dish. For a given lipid composition, ~100 GUVs were observed and scored based on whether they have undergone influx of Alexa Fluor 488. As a positive control for poration, the pore forming peptide melittin was added to a suspension of POPC GUVs at 1:50 peptide-to-lipid ratio.

Confocal microscopy

GUVs were imaged on a Zeiss LSM 880 microscope using a 63x oil 1.4 NA Plan-Apochromat objective. The objective was connected to an objective heater (Bioptechs, Butler, PA) to maintain 37 ^{0}C inside the chamber (chamber temperature was verified with a microprobe). Alexa Fluor 488, R-18 and DiD were excited with 488, 543 and 633 nm lasers respectively and detected using PMT detectors on separate tracks.

Image, data and statistical analyses

Microscopy images were analyzed using ImageJ (NIH). Data were analyzed using SigmaPlot (Systat Software, Inc., Chicago, IL), Excel (Microsoft, Inc., Redmond, WA), and MATLAB (The MathWorks, Inc., Natick, MA).

Journal of Cell Science • Accepted manuscript

Acknowledgments

The authors thank Petr Chlanda and Matthias Garten for helpful discussions.

Competing interests

The authors declare no competing or financial interests

Author contributions

The project was planned by S.H., P.S.B. and J.Z. Experimental work was performed by S.H. E.M. generated virus and purified them. C.D.M. assisted with microscopy and image processing. Statistical analysis and modelling was performed by P.S.B. The manuscript was written by S.H., P.S.B. and J.Z. All authors assisted in editing the manuscript.

Funding

This work was supported by the Division of Intramural Research of the Eunice Kennedy Shriver National Institute of Child Health and Human Development.

Journal of Cell Science • Accepted manuscript

REFERENCES

Arbuzova, A., Korte, T., Muller, P. and Herrmann, A. (1994). On the validity of lipid dequenching assays for estimating virus fusion kinetics. *Biochim. Biophys. Acta* **1190**, 360-366.

Bao, H., Goldschen-Ohm, M., Jeggle, P., Chanda, B., Edwardson, J. M. and Chapman, E. R. (2016). Exocytotic fusion pores are composed of both lipids and proteins. *Nat. Struct. Mol. Biol.* **23**, 67-73.

Blank, P. S., Vogel, S. S., Malley, J. D. and Zimmerberg, J. (2001). A kinetic analysis of calcium-triggered exocytosis. *J. Gen. Physiol.* **118**, 145-156.

Bleicken, S., Wagner, C. and Garcia-Saez, A. J. (2013). Mechanistic differences in the membrane activity of Bax and Bcl-xL correlate with their opposing roles in apoptosis. *Biophys. J.* **104**, 421-431.

Blumenthal, R. and Morris, S. J. (1999). The influenza haemagglutinin-induced fusion cascade: effects of target membrane permeability changes. *Mol. Membr. Biol.* **16**, 43-47.

Bonnafous, P. and Stegmann, T. (2000). Membrane perturbation and fusion pore formation in influenza hemagglutinin-mediated membrane fusion. A new model for fusion. *J. Biol. Chem.* **275**, 6160-6166.

Chernomordik, L. (1996). Non-bilayer lipids and biological fusion intermediates. *Chem. Phys. Lipids* **81**, 203-213.

Chernomordik, L. V., Frolov, V. A., Leikina, E., Bronk, P. and Zimmerberg, J. (1998). The pathway of membrane fusion catalyzed by influenza hemagglutinin: restriction of lipids, hemifusion, and lipidic fusion pore formation. *J. Cell. Biol.* **140**, 1369-1382.

Chernomordik, L. V., Kozlov, M. M., Melikyan, G. B., Abidor, I. G., Markin, V. S. and Chizmadzhev, Y. A. (1985). The Shape of Lipid Molecules and Monolayer Membrane-Fusion. *Biochim. Biophy. Acta* **812**, 643-655.

Chernomordik, L. V., Leikina, E., Frolov, V., Bronk, P. and Zimmerberg, J. (1997). An early stage of membrane fusion mediated by the low pH conformation of influenza hemagglutinin depends upon membrane lipids. *J. Cell. Biol.* **136**, 81-93.

Chernomordik, L. V., Leikina, E., Kozlov, M. M., Frolov, V. A. and Zimmerberg, J. (1999). Structural intermediates in influenza haemagglutinin-mediated fusion. *Mol. Membr. Biol.* **16**, 33-42.

Chernomordik, L. V. and Zimmerberg, J. (1995). Bending membranes to the task: structural intermediates in bilayer fusion. *Curr. Opin. Struct. Biol.* **5**, 541-547.

Chernomordik, L. V., Zimmerberg, J. and Kozlov, M. M. (2006). Membranes of the world unite! *J. Cell. Biol.* **175**, 201-217.

Chlanda, P., Carbajal, M. A., Cyrklaff, M., Griffiths, G. and Krijnse-Locker, J. (2009). Membrane rupture generates single open membrane sheets during vaccinia virus assembly. *Cell Host Microbe* **6**, 81-90.

Chlanda, P., Mekhedov, E., Waters, H., Schwartz, C. L., Fischer, E. R., Ryham, R. J., Cohen, F. S., Blank, P. S. and Zimmerberg, J. (2016). The hemifusion structure induced by influenza virus haemagglutinin is determined by physical properties of the target membranes. *Nat. Microbiol.* **1**, 16050

Coorssen, J. R., Blank, P. S., Tahara, M. and Zimmerberg, J. (1998). Biochemical and functional studies of cortical vesicle fusion: the SNARE complex and Ca2+ sensitivity. *J. Cell. Biol.* **143**, 1845-1857.

Journal of Cell Science • Accepted manuscript

Engel, A. and Walter, P. (2008). Membrane lysis during biological membrane fusion: collateral damage by misregulated fusion machines. *J. Cell. Biol.* **183**, 181-186.

Evans, E. and Needham, D. (1986). Giant vesicle bilayers composed of mixtures of lipids, cholesterol and polypeptides. Thermomechanical and (mutual) adherence properties. *Faraday Discuss. Chem. Soc.***81**, 267-280.

Foster, K. A., Gill, K., Micklem, K. J. and Pasternak, C. A. (1980). Survey of virally mediated permeability changes. *Biochem. J.* **190**, 639-646.

Frolov, V. A., Dunina-Barkovskaya, A. Y., Samsonov, A. V. and Zimmerberg, J. (2003). Membrane permeability changes at early stages of influenza hemagglutinin-mediated fusion. *Biophys. J.* **85**, 1725-1733.

Gui, L., Ebner, J. L., Mileant, A., Williams, J. A. and Lee, K. K. (2016). Visualization and Sequencing of Membrane Remodeling Leading to Influenza Virus Fusion. *J. Virol.* **90**, 6948-6962.

Hamilton, B. S., Whittaker, G. R. and Daniel, S. (2012). Influenza virus-mediated membrane fusion: determinants of hemagglutinin fusogenic activity and experimental approaches for assessing virus fusion. *Viruses* **4**, 1144-1168.

Karatekin, E., Sandre, O., Guitouni, H., Borghi, N., Puech, P. H. and Brochard-Wyart, F. (2003). Cascades of transient pores in giant vesicles: line tension and transport. *Biophys. J.* **84**, 1734-1749.

Katsov, K., Muller, M. and Schick, M. (2006). Field theoretic study of bilayer membrane fusion: II. Mechanism of a stalk-hole complex. *Biophys. J.* **90**, 915-926.

Kollmitzer, B., Heftberger, P., Rappolt, M. and Pabst, G. (2013). Monolayer spontaneous curvature of raft-forming membrane lipids. *Soft Matter* **9**, 10877-10884.

Lee, K. K. (2010). Architecture of a nascent viral fusion pore. *EMBO J.* **29**, 1299-1311.

Lee, M. T., Hung, W. C., Chen, F. Y. and Huang, H. W. (2008). Mechanism and kinetics of pore formation in membranes by water-soluble amphipathic peptides. *Proc. Natl. Acad. Sci. U S A* **105**, 5087-5092.

Longo, M. L., Waring, A. J. and Hammer, D. A. (1997). Interaction of the influenza hemagglutinin fusion peptide with lipid bilayers: area expansion and permeation. *Biophys. J.***73**, 1430-1439.

Melikyan, G. B., Brener, S. A., Ok, D. C. and Cohen, F. S. (1997). Inner but not outer membrane leaflets control the transition from glycosylphosphatidylinositol-anchored influenza hemagglutinin-induced hemifusion to full fusion. *J. Cell. Biol.* **136**, 995-1005.

Muller, M., Katsov, K. and Schick, M. (2003). A new mechanism of model membrane fusion determined from Monte Carlo simulation. *Biophys. J.* **85**, 1611-1123.

Murata, M., Takahashi, S., Kagiwada, S., Suzuki, A. and Ohnishi, S. (1992). pH-dependent membrane fusion and vesiculation of phospholipid large unilamellar vesicles induced by amphiphilic anionic and cationic peptides. *Biochemistry* **31**, 1986-1992.

Needham, D. and Nunn, R. S. (1990). Elastic deformation and failure of lipid bilayer membranes containing cholesterol. *Biophys. J.* **58**, 997-1009.

Palade, G. (1975). Intracellular aspects of the process of protein synthesis. *Science* **189**, 867.

Papanicolaou, K. N., Phillippo, M. M. and Walsh, K. (2012). Mitofusins and the mitochondrial permeability transition: the potential downside of mitochondrial fusion. *Am J Physiol Heart Circ Physiol* **303**, H243-H255.

Journal of Cell Science • Accepted manuscript

Pasternak, C. A. and Micklem, K. J. (1981). Virally induced alterations in cellular permeability: a basis of cellular and physiological damage? *Biosci. Rep.* **1**, 431-448.

Risselada, H. J., Bubnis, G. and Grubmuller, H. (2014). Expansion of the fusion stalk and its implication for biological membrane fusion. *Proc. Natl. Acad. Sci. U S A* **111**, 11043-8.

Risselada, H. J. and Grubmuller, H. (2012). How SNARE molecules mediate membrane fusion: recent insights from molecular simulations. *Curr Opin Struct Biol* **22**, 187-196.

Ryham, R. J., Klotz, T. S., Yao, L. and Cohen, F. S. (2016). Calculating Transition Energy Barriers and Characterizing Activation States for Steps of Fusion. *Biophys. J.* **110**, 1110-24.

Shah, P., Wolf, K. and Lammerding, J. (2017). Bursting the Bubble - Nuclear Envelope Rupture as a Path to Genomic Instability? *Trends Cell. Biol.* **27**, 546-555.

Shangguan, T., Alford, D. and Bentz, J. (1996). Influenza-virus-liposome lipid mixing is leaky and largely insensitive to the material properties of the target membrane. *Biochemistry* **35**, 4956-4965.

Smrt, S. T. and Lorieau, J. L. (2017). Membrane Fusion and Infection of the Influenza Hemagglutinin. *Adv. Exp. Med. Biol.* **966**, 37-54.

Soltesz, S. A. and Hammer, D. A. (1995). Micropipette manipulation technique for the monitoring of pH-dependent membrane lysis as induced by the fusion peptide of influenza virus. *Biophys. J.* **68**, 315-325.

Szule, J. A., Fuller, N. L. and Rand, R. P. (2002). The effects of acyl chain length and saturation of diacylglycerols and phosphatidylcholines on membrane monolayer curvature. *Biophys. J.* **83**, 977-984.

Vogel, S. S., Blank, P. S. and Zimmerberg, J. (1996). Poisson-distributed active fusion complexes underlie the control of the rate and extent of exocytosis by calcium. *J. Cell. Biol.* **134**, 329-338.

Weinberger, A., Tsai, F. C., Koenderink, G. H., Schmidt, T. F., Itri, R., Meier, W., Schmatko, T., Schroder, A. and Marques, C. (2013). Gel-assisted formation of giant unilamellar vesicles. *Biophys. J.***105**, 154-164.

White, J. M. and Whittaker, G. R. (2016). Fusion of Enveloped Viruses in Endosomes. *Traffic* **17**, 593-614.

Young, J. D., Young, G. P., Cohn, Z. A. and Lenard, J. (1983). Interaction of enveloped viruses with planar bilayer membranes: observations on Sendai, influenza, vesicular stomatitis, and Semliki Forest viruses. *Virology* **128**, 186-194.

Zimmerberg, J., Blank, P. S., Kolosova, I., Cho, M. S., Tahara, M. and Coorssen, J. R. (2000). A stage-specific preparation to study the Ca(2+)-triggered fusion steps of exocytosis: rationale and perspectives. *Biochimie* **82**, 303-314.

Journal of Cell Science • Accepted manuscript

Table 1

Lipid compositions and corresponding lipid monolayer spontaneous curvature. Spontaneous curvatures of lipid mixtures were estimated by mole fraction weighted addition of spontaneous curvature individual lipids. Note, we ignored the contribution of 5 mol % total ganglioside (TG) to our estimate of spontaneous curvature.

Monolayer Spontaneous Curvature $J = \sum J_i \varphi_i$ nm^{-1} (J_i = Sp. Cur. and φ_i = mole fraction of individual lipids)	**POPC:CHOL:TG**	**PC:PE:TG**	**PC:DOG:TG**	**PC:CHOL:PE:TG**
-0.022	**95:00:05**	**95:00:05**	**95:00:05**	**95:0:0:5**
-0.116	**75:20:05**	**63:32:05**	**85:10:05**	
-0.134				**66:16:13:5**
-0.164	**65:30:05**	**47:48:05**	**80:15:05**	
-0.211	**55:40:05**	**31:64:5**	**76:19:05**	
-0.243		**20:75:5**	**71:24:05**	**42:40:13:5**
-0.258	**45:50:05**	**15:80:5**		
-0.281	**40:55:05**			
-0.305	**35:60:5**		**66:29:05**	

Journal of Cell Science • Accepted manuscript

Figures

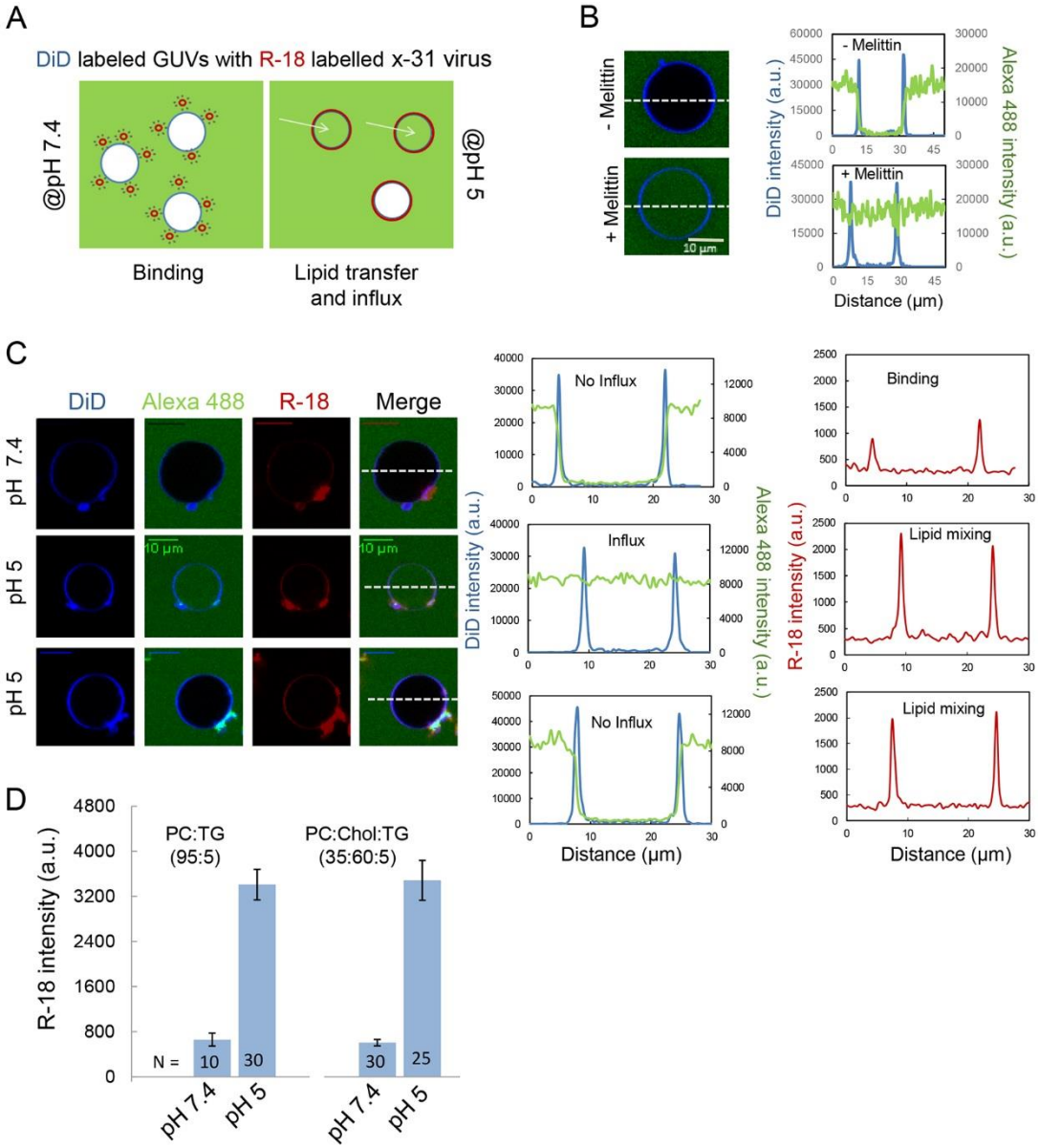

Journal of Cell Science • Accepted manuscript

Fig. 1. Poration assay. (A) Scheme of the experiment. Giant Unilamellar Vesicles (GUV) with desired lipid compositions labelled with DiD (blue) were incubated with R-18 labelled X-31 influenza virus (red) at 37 ^{0}C for 30 min in pH 7.4 buffer containing Alexa-488 (green). This was followed by a change in pH 7.4 to pH 5. After 10 minutes of incubation at pH 5, numbers of filled (Alexa-488 positive) and unfilled (Alexa-488 negative) vesicles were counted. See materials and methods for details. (B) Poration of GUVs. Influx of Alexa-488 (green) to POPC GUVs in presence of pore-forming peptide melittin. Line profile in green indicates intensity distribution Alexa-488 in the absence and presence of melittin. Blue profile indicates DiD intensity. (C) Representative examples of leakage (dye influx) and lipidic-dye transfer from viral to GUV membranes. Images shown are confocal section GUV equatorial planes. Intensity profiles of DiD (blue), Alexa-488 (green) and R-18 (red) along the radial axis of GUVs (dotted line). Line profile in green channel indicates leakage and in red channel indicates lipidic dye transfer. (d) Average intensity of R-18 along the radial distance at pH 7.4 and pH 5. Error bars represent SEM (sample size (N=) is indicated in the Fig.) Note the increase in intensity due to lipid transfer (hemi-fusion) between viral and GUV membranes and consequent dequenching due to dye transfer from viral to the target membrane. See methods section for details. Scale bars 10 µm.

Journal of Cell Science • Accepted manuscript

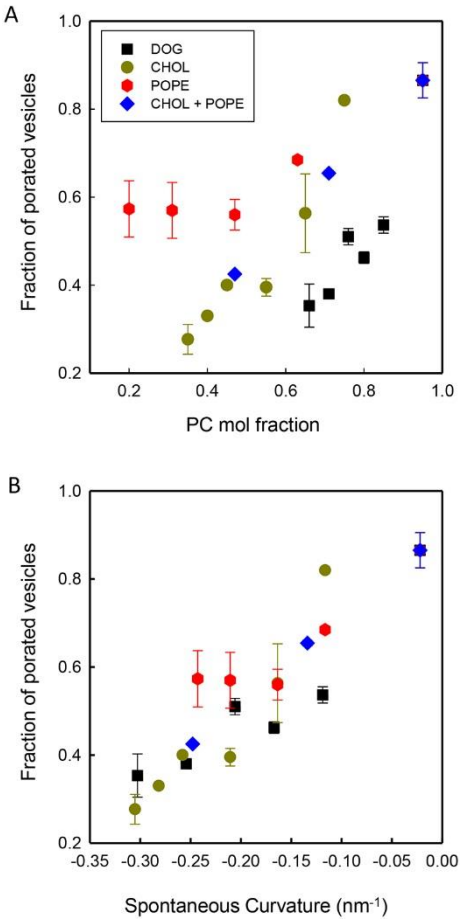

Fig. 2. Dependence of Poration. (A) Dependence of leakage on the concentration of non-bilayer forming lipids in bilayer. Fractions of filled GUVs are plotted against the POPC mol fraction of target membranes. POPC mole fraction decreases as the mole fraction of non-bilayer forming lipids characterized by negative spontaneous curvature increases (see Table 1). (B) Variation of leakage with spontaneous curvature. Spontaneous curvature values were obtained by linear combination of constituent lipids (in Fig. 2A) weighted by their mole fraction. See Table 1 for details of the compositions. Typically, 100 vesicles are counted in each case and error bars represent SEM of at least three independent measurements. Note that individual lipid series tend to converge on the spontaneous curvature axis.

Journal of Cell Science • Accepted manuscript

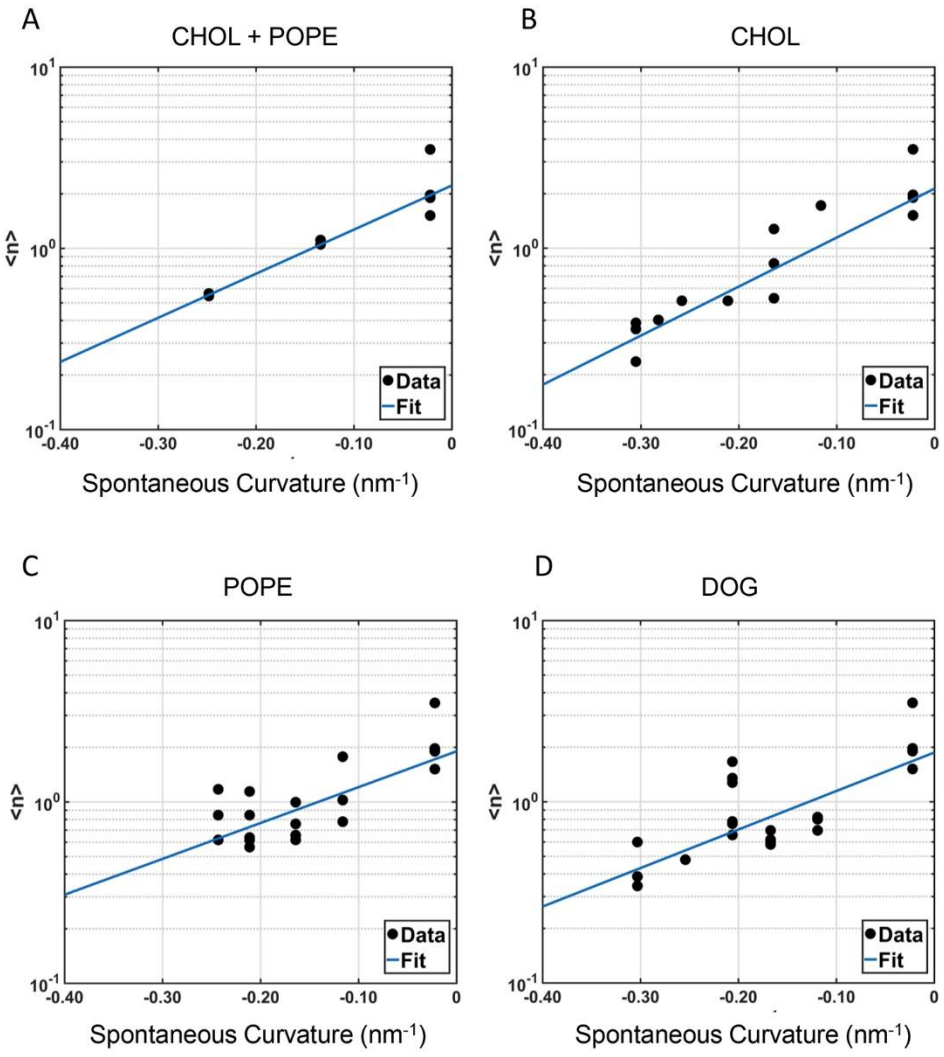

Fig. 3. Poisson analysis. <n> analysis of lipid compositions showing the postulated exponential relationship (linear on a log scale) between Poisson-distributed "leakage machines" and spontaneous curvature for (A) POPC:CHOL:POPE:TG (B) POPC:CHOL:TG (C) POPC:POPE:TG and (D) POPC:DOG:TG. See main text and Table 1 for lipid compositions and Supplementary Information for analysis and fitting parameters.

Journal of Cell Science • Accepted manuscript

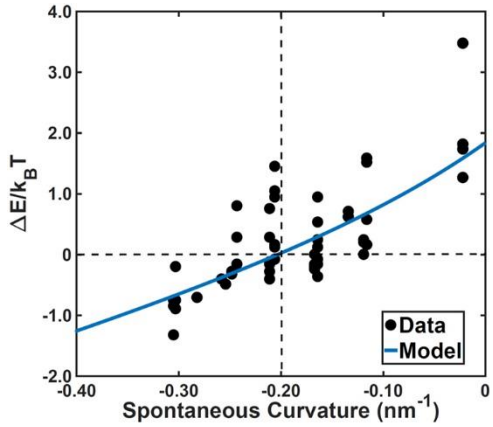

Fig. 4. Energetics analysis. Poisson leakage model expressed as energy changes using the probabilities for leakage and no-leakage and the calculated energy changes derived from the measured leakage fraction. ΔE (phenomenological energy difference between leaky and non-leaky) was obtained by Boltzmann analysis of the probabilities of occurrence of leaky versus non-leaky vesicles. The energy crossover point occurs at SC $\sim -0.2\ \mathrm{nm}^{-1}$. Lipid composition of cumulative spontaneous curvature $> -0.21\ \mathrm{nm}^{-1}$ corresponds to the leaky 'rupture-insertion' regime while $< -0.21\ \mathrm{nm}^{-1}$ corresponds to the non-leaky 'hemifusion-stalk' regime. Target membrane with lipid composition corresponding to the rupture-insertion regime is likely to exhibit content leakage or influx.

Journal of Cell Science • Accepted manuscript

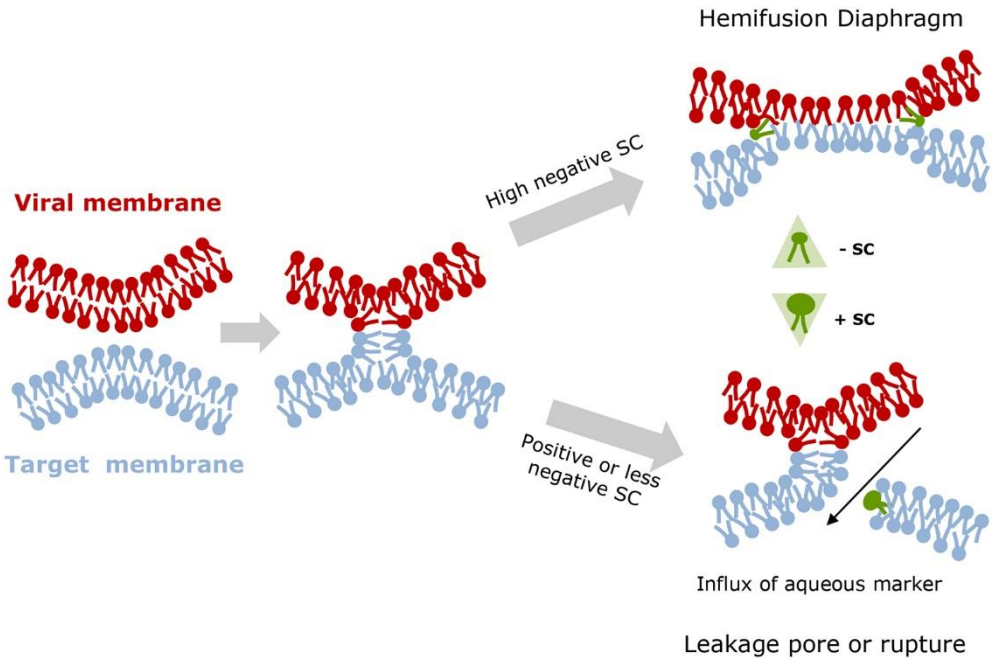

Fig. 5. A cartoon representation of the possible interaction between the viral and the target membrane. In the presence of lipids with negative spontaneous curvature of the monolayer in the target membrane, stalk formation is favored. Since the perimeter of a stalk is negative, it is stabilized in the presence of lipids with negative spontaneous curvature (cone-shaped lipids, shown in the cartoon) of the monolayer and can extend to form a hemifusion diaphragm. The hemifusion diaphragm eventually forms the fusion pore merging the two compartments initially separated by the viral and the target membranes. On the other hand, when the spontaneous curvature of the contacting monolayer of the target membrane is less negative or positive, stalk formation and elongation is not favored energetically, and the target membrane ruptures to form a leakage pore. A leakage pore (in the target membrane) does not connect the two compartments but causes efflux of contents from the target membrane or influx of aqueous markers (as detected in the current assay). A leakage pore may have similar topology of a fusion pore (positive curvature at the edge) which is stabilized in the presence of lipids with positive (or less negative) spontaneous curvature

Journal of Cell Science • Accepted manuscript

of the monolayer (inverse cone-shaped lipids, shown in the cartoon). Note that in our current assay fusion pore formation was not monitored and only the probability of leakage pore formation had been determined.

Journal of Cell Science • Accepted manuscript

Table S1: Parameters of the fit (Fig. 3), are (to a first approximation) statistically the same using the 95% confidence bounds. However, there are differences in the goodness of fit parameters between the compositions containing POPC:POPE:TG (20 measurements) and POPC:DOG:TG (21 measurements) when compared with POPC:CHOL:POPE:TG (12 measurements) and POPC:CHOL:TG (15 measurements). The fitting results are summarized.

Lipid Compositions	Coefficients (with 95% confidence bound)		Goodness of fit			
	a	b	SSE	R^2	Reduced R^2	RMSE
POPC:CHOL:POPE:TG	2.23 (1.89, 2.56)	5.61 (3.81, 7.40)	0.58	0.93	0.92	0.24
POPC:CHOL:TG	2.14 (1.78, 2.45)	6.23 (4.36, 8.11)	0.87	0.93	0.92	0.26
POPC:POPE:TG	1.90 (1.45, 2.36)	4.55 (2.58, 6.53)	2.27	0.76	0.75	0.36
POPC:DOG:TG	1.87 (1.40, 2.34)	4.89 (2.82, 6.97)	2.64	0.76	0.75	0.37
All data	1.99 (1.82, 2.16)	5.18 (4.39, 5.97)	5.04	0.88	0.87	0.28

Journal of Cell Science • Supplementary information

Table S1: Parameters of the fit (Fig. 3), are (to a first approximation) statistically the same using the 95% confidence bounds. However, there are differences in the goodness of fit parameters between the compositions containing POPC:POPE:TG (20 measurements) and POPC:DOG:TG (21 measurements) when compared with POPC:CHOL:POPE:TG (12 measurements) and POPC:CHOL:TG (15 measurements). The fitting results are summarized.

Lipid Compositions	Coefficients (with 95% confidence bound)		Goodness of fit			
	a	b	SSE	R^2	Reduced R^2	RMSE
POPC:CHOL:POPE:TG	2.23 (1.89, 2.56)	5.61 (3.81, 7.40)	0.58	0.93	0.92	0.24
POPC:CHOL:TG	2.14 (1.78, 2.45)	6.23 (4.36, 8.11)	0.87	0.93	0.92	0.26
POPC:POPE:TG	1.90 (1.45, 2.36)	4.55 (2.58, 6.53)	2.27	0.76	0.75	0.36
POPC:DOG:TG	1.87 (1.40, 2.34)	4.89 (2.82, 6.97)	2.64	0.76	0.75	0.37
All data	1.99 (1.82, 2.16)	5.18 (4.39, 5.97)	5.04	0.88	0.87	0.28

Journal of Cell Science • Supplementary information